Chem Rev Lett 7 (2024) 701-711

Research Article

Chemical Review and Letters
journal homepage: www.chemrevlett.com
ISSN (online): 2645-4947 (print) 2676-7279

Influence of graphene oxide on the catalytic activity of Fe_3O_4 nanoparticles

Robab Mohammadi[1, *], Rovnag Rzayev[2]

[1]*Department of Chemistry, Payame Noor University, PO box 19395-3697, Tehran, Iran*
[2]*Composite Materials Scientific Research Center of Azerbaijan State University of Economic (UNEC), 194 M.Mukhtarov str. Baku, Azerbaijan*

ARTICLE INFO

Article history:
Received 14 June 2024
Received in revised form 16 August 2024
Accepted 18 August 2024
Available online 9 September 2024

Keywords:
Fe_3O_4/Graphene oxide,
Photodegradation,
Sonodegradation,
Graphene content,
Kinetic model.

ABSTRACT

In this research, a series of Fe_3O_4 and Fe_3O_4/Graphene oxide nanocompounds with various contents of graphene in the composite were prepared using iron chloride and graphene oxide as the starting materials. The synthesized Fe_3O_4/Graphene oxide was characterized by XRD, SEM, EDX, FT-IR, and UV–visible spectroscopy. The photocatalytic and sonocatalytic activities of the synthesized samples were investigated by the degradation of malachite green as a cationic dye. Fe_3O_4/Graphene oxide was found to be more efficient at photodegradation of malachite green. The photodegradation reaction fit well to a Langmuir-Hinshelwood kinetic model implying the reaction rate is depended on initial adsorption step. The quantities of the adsorption equilibrium constant (K_{dye}) and the kinetic rate constant of surface reaction (k_c) were 0.91 (mg L^{-1})$^{-1}$ and 2.32 mg L^{-1} min^{-1}, respectively. Based on results, the rate constant of sonocatalysis was higher than that of photocatalysis. Finally, it has been concluded that graphene when employed as catalytic support for Fe_3O_4 increases its catalytic activity.

1. Introduction

The development of the textile and dyeing industries has led to enhance levels of water pollution, with organic pollutants contributing significantly to this pollution [1]. Different techniques have been designed to remove the dye pollutants from wastewater, such as adsorption, extraction, ultrafiltration/nanofiltration, coagulation/ flocculation, electrochemical reduction, and advanced oxidation procedures (AOPs) [2]. In past decades, advanced oxidation procedures (AOPs) are known as the most suitable technologies for the treatment of water. This method usually involves light-trapping heterogeneous catalysts that contact organic dyes pollutants in a solution, thereby decomposing the structure of dangerous dyes into environmentally benign materials under the irradiation of the UV or visible light [3]. Notably, iron (Fe)-based heterogeneous catalyst materials (e.g., Fe_3O_4) are regarded as promising candidates for AOPs procedures due to their high natural abundance, low price, and they could easily inhibit secondary pollution through their recovery performance [4, 5]. However, Fe_3O_4 nanoparticles may aggregate in the solution, which can decline their surface area and cause lower stability and catalytic efficiency [6]. Thus, it is necessary to apply a proper support that can increase their overall performance. Graphene has been widely reported to be an emerging supporting material for metal oxides [7]. More recently, there are lots of research on graphene with good qualities, such as strongest mechanical strength, fast electron mobility rate, specific surface, adsorption capacity, and potentially higher photocatalytic efficiencies [8]. To improve its dissolving property, graphene is modified by oxidization into graphene oxide (GO) [9]. Large porous graphene sheets have the potential to adsorb more quantities of dyes on their surface, and inhibit selective adsorption for desired pollutants. Some functional groups such as alcohol and carboxylic acids can be remained on the graphene surface during synthesize process [10], allowing for both adsorption of specific pollutants and attachment sites for nanoparticles to the graphene surface. So, different catalysts can be stabilized on its surface to produce more major photocatalysts [11]. However, graphene needs

∗ Corresponding author; e-mail: mohammadi_rb@yahoo.com, r.mohammadi@pnu.ac.ir
https://doi.org/10.22034/crl.2024.461585.1355

additional treatment procedure for its application in practical usages because of graphene's tendency to agglomerate by van der Waals interactions, which decreases graphene's unique properties. To enhance graphene's advantageous properties and to reduce its stacking procedure, different types of graphene structures have been investigated, such as functionalized graphene, N-doped graphene, graphene-polymer composites and graphene-metal composites. Based on researches, graphene-metal composites demonstrate unique properties as a result of their synergistic influences. Metal nanoparticles can affect the structure and characteristics of graphene in two basic ways: (1) metal nanoparticles reduce the generation of the graphene aggregate structure via permeating the interface between the structural layers of the graphene and (2) metal nanoparticles decorate the graphene surface through chemical or physical interactions to great material that demonstrates outstanding multifunctional properties. Fe_3O_4 has widespread availability, is eco-friendly, has a high theoretical capacity and has strong superparamagnetism. Fe_3O_4/Graphene oxide nanocomposite, which demonstrates special magnetic and super capacitance properties, has attracted much attention for energy and environmental usages, including for application in lithium ion batteries, as a catalyst and in magnetic separations [12].

For the last two decades, application of ultrasound in materials synthesis has been a very promising topic e specially for the fabrication or modification of various n anomaterials [13].

he physical phenomenon essential for sonochemica l process is largely accepted owing to acoustic cavitatio n, involving formation, growth, and implosive collapse of the micro-
bubbles inside liquid. The resulting hot spots/microjets generate very high temperatures ~5000 K and high pres sure ~150 MPa due to collapsing bubbles within a nano second, with high cooling rates exceeding 10^{11} Ks^{-1} at t he local reaction centre, providing necessary activation for faster kinetics [14]. Sonocatalytic process, which is a combination of catalyst with ultrasonic has gotten more attention recently. The sonocatalytic performance to remove organic dyes can be increased due to a synergistic effect of ultrasonicradiation with a solid catalyst [15].

The aim of the present research was to prepare Fe_3O_4 and Fe_3O_4/Graphene oxide magnetic nanocompounds and investigate the effect of graphene in the degradation of malachite green as a pollutant model. To understand which energy source is better in terms of the synergistic influence with Fe_3O_4/Graphene oxide nanocomposite for the degradation of malachite green, UV-A light and US waves were applied as sources of energy. In addition, the photodegradation and sonodegradation mechanisms of malachite green on Fe_3O_4/Graphene oxide nanocomposite were investigated. The proposed mechanism of malachite green sonodegradation includes the sonochemical oxidation of malachite green molecules by $OH^{\cdot}$ /HO_2 radicals in solution and malachite green oxidation at the surface of Fe_3O_4/Graphene oxide nanocomposite in the presence of O_2 activated via the cavitation event. These results are being compared herein with those of the photocatalytic malachite green degradation results.

2. Experimental Section

2.1 Materials and Methods

Iron (III) chloride hexahydrate ($FeCl_3 \cdot 6H_2O$), Iron (II) chloride tetrahydrate ($FeCl_2 \cdot 4H_2O$), ammonium hydroxide (28% v/v, $NH_3 \cdot H_2O$), graphite powder (purity 99.999%), nitric acid, sulfuric acid, potassium chlorate, sodium hydroxide and malachite green were purchased from Merck Co (Germany).

2.1.1 Preparation of Fe_3O_4 nanoparticles

Fe_3O_4 nanoparticles were synthesized by reverse co precipitation method using ammonia as precipitation agent. In short, 5 mL of 1 mol L^{-1} $FeCl_3.6H_2O$ solution and 10 mL of 0.5 mol L^{-1} $FeCl_2.4H_2O$ solutions were mixed. The mixture was added drop wise into 20 mL of 3.5 mol L^{-1} ammonium hydroxide solution at 60 °C under ultrasound irradiation. The reaction proceeded for 30 min. Upon completion of the reaction, the resulting black iron oxide nanoparticles were collected with the help of a strong magnet and washed several times with distilled water.

2.1.2 Preparation of Graphene oxide sample

Graphene was synthesized via Staudenmaier method. Briefly, 5 g graphite was reacted with 45 mL concentrated nitric acid and 90 mL sulfuric acid and 55 g potassium chlorate. To inhibit any sudden enhancement in temperature, the potassium chlorate was gradually added under constant stirring for 30 min and mixture was stirred for 72 h at room temperature. The mixture was added to water after completing the reaction, washed with a 5% solution of HCl, and deionized water repeatedly until the pH of the filtrate was neutral. The dried graphene was placed in a quartz boat and inserted into a tubular furnace preheated to 1050 °C and kept at this temperature for 30 s.

2.1.3 Preparation of Fe_3O_4 and Fe_3O_4/Graphene oxide materials

Fe_3O_4/Graphene oxide materials were synthesized via co-precipitating pre-hydrolyzed ferric and ferrous salts in the presence of Graphene. An aqueous solution (100 mL) containing $FeCl_3 \cdot 6H_2O$ (4 mmol) and ($FeCl_2 \cdot 4H_2O$ (2 mmol)) was synthesized with an initial pH of 1.48 and subsequently adjusted to pH 4 by addition of NaOH (1 M). 5 mg of Graphene was dissolved in a solution of 90 mL distilled water and 30 mL ethanol by ultrasonic treatment for 2 h and gradually added into the iron oxide solution under constant stirring for 30 min. The pH was adjusted to 10 via adding NaOH (1 M) to the mixture which was then aged at constant stirring for a further 40 min at room temperature. The resulting black precipitate was magnetically separated and washed three times with deionized water and ethanol followed by drying for 48 h in an oven at 70 ° C. The synthesized sample was designated as Fe_3O_4/Graphene $oxide_1$. Similar method was used to prepare other Fe_3O_4/Graphene oxide catalysts via fixing the amount of Fe_3O_4 and using 10, 20 and 30 mg of graphene respectively. The synthesized catalysts were designated as Fe_3O_4/Graphene $oxide_2$, Fe_3O_4/Graphene $oxide_3$, and Fe_3O_4/Graphene $oxide_4$ respectively. The best catalyst procured in this method was designated as Fe_3O_4/Graphene oxide.

2.2 Catalytic experiment

Degradation of malachite green under black light illumination was applied as a model reaction to investigate the photocatalytic activity of prepared catalysts. Photocatalytic activity measurements were evaluated at atmospheric pressure in a batch quartz reactor. Artificial illumination was provided via 36 W (UV-A) mercury lamp (Philips, Holland) emitted around 620 nm positioned above the batch photoreactor.

In each run, 40 mg of prepared sample and desired amount of methyl red were fed into the batch quartz reactor and placed in the dark condition for 30 min with continuous stirring for adsorption–desorption equilibrium and then exposed to black-light irradiation. The zero time reading was obtained from blank solution kept in the dark. The photocatalytic reaction was then started by irradiating the suspension with black light. Every 4 min as interval time, 5 mL of the pollutant suspension was withdrawn and centrifuged to remove catalyst particles. The concentration of remaining methyl red was detected via UV–Vis Perkin–Elmer 550 SE spectrophotometer at the wavelength of 465 nm.

All the concentration profiles may be correlated to illumination time via the following exponential function with good agreement:

$$\frac{-d[C]}{dt} = k_{obs}\,[C] \qquad (1)$$

So, the catalytic degradation of malachite green is pseudo-first-order reaction, and its kinetics can also be expressed as:

$$Ln\,\frac{[C]_0}{[C]} = k_{obs}\,t \qquad (2)$$

In this equation, $[C]_0$ and $[C]$ are the pollutant concentrations (mg L^{-1}) at times 0 and *t*, respectively, and k_{obs} is the pseudo-first-order rate constant (min^{-1}).

3. Results and Discussion

3.1 Characterization of prepared nanocomposite

3.1.1 X-ray diffraction (XRD)

The XRD pattern of the synthesized Fe_3O_4/Graphene oxide nanocomposite with typical characteristics is shown in Figure 1. For graphene oxide (Figure is not shown), there was only a broad peak at 2θ = 10.6° assigned to the (002) plane. This is attributed to interaction of water molecules and generation of oxygenated functional groups such as epoxy and hydroxyl groups between the inter-galleries of the graphite sheets during severe oxidation [16]. For Fe_3O_4/Graphene oxide nanocomposite, each diffraction peak of the catalyst can be assigned to the cubic phase structure (JCPDS card, file no. 79-0418). The peaks at 2Θ values: 29.7, 35.5, 43.1, 53. 1, 57.1, 62.2 and 74.1° could be indexed as the (220), (311), (400), (422), (511), (440) and (553) crystal planes of cubic phase Fe_3O_4, respectively *[13]*. The sharpness of the peaks clearly implies that the synthesized particles had a highly crystalline nature. These crystalline entities show the typical pattern of Fe_3O_4, and there was no other phase such as Fe_2O_3 or $Fe(OH)_3$, which were the usual co-products in chemical reverse coprecipitation process. Disappearance of the reflection plane at (002) and merging of the planes of Fe_3O_4 show the good interfacial interaction between the planes, and confirm the complete reduction of graphene. The crystallite size of prepared particle, according to the FWHM of the (311) plane refraction peak, was calculated by the Debye-Scherrer formula through equation:

$$D = \frac{k\lambda}{\beta\cos\theta} \qquad (3)$$

Where K is the shape factor, λ is the X-ray wavelength (0.154 nm), β is the line broadening at half the maximum intensity (FWHM) in radian, and θ is the Bragg angle [17-18]. D (in nm) is the mean size of the

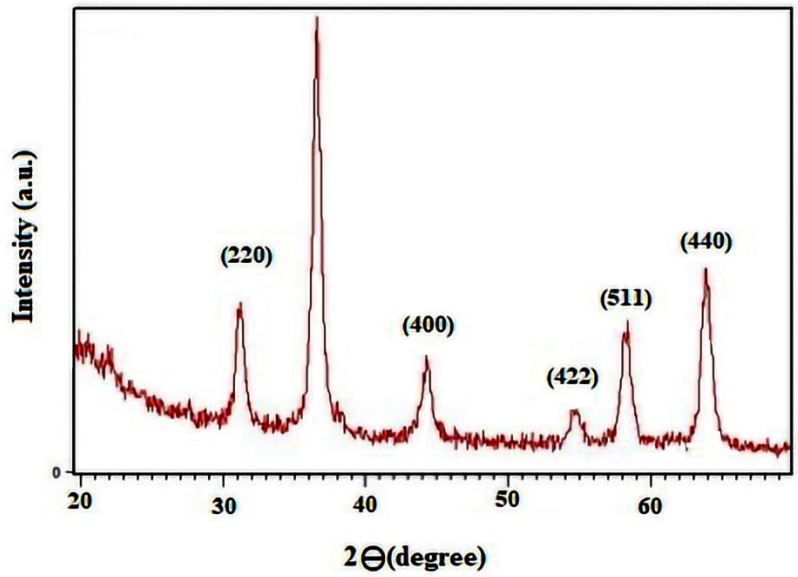

Fig. 1. XRD pattern of Fe_3O_4/Graphene oxide nanocomposite.

ordered (crystalline) domains that may be smaller or equal to the grain size. The crystallite size thus obtained from this equation was found to be about 16 nm.

3.1.2 SEM analysis of Fe_3O_4/Graphene oxide nanocomposite

SEM image was applied to study the morphology and aggregation level of materials. Fig. 2 illustrates SEM image of Fe_3O_4/Graphene oxide nanocomposite. As can be observed that, SEM image shows particles with good homogeneity, granular structure and slight agglomeration. Since less particle agglomeration occurred for Fe_3O_4/Graphene oxide nanocomposite, the large surface area conveys high adsorption capacities of this material [19].

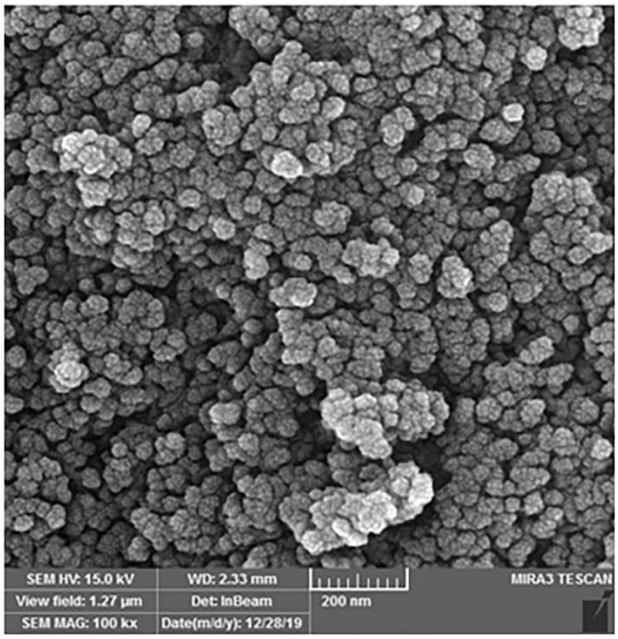

Fig. 2. SEM image of Fe_3O_4/Graphene oxide nanocomposite.

3.1.3 FTIR spectrum of Fe_3O_4/Graphene oxide nanocomposite

The FTIR spectrum of Fe_3O_4/Graphene oxide nanocomposite is shown in Fig. 3. The 788 and 580 cm^{-1} absorption peaks correspond to the Fe–O bond vibration of Fe_3O_4 nanoparticles [20]. The peak at 1385 cm^{-1} is related to the C-O-C stretching vibrations. The bands at 1602 cm^{-1} and 1438 cm^{-1} are associated with the asymmetric and symmetric vibration of COO^- groups, respectively. The band at 2850 and 2920 cm^{-1} are assigned to the stretch vibration absorption of aliphatic C-H [21]. The absorbance peak around 3300-3362 cm^{-1} is attributed to the stretching of O–H. Results showed that when the graphite is oxidized, it will modify at least four functional groups, such as OH, COOH, C=O, and C-O-C. These polar groups contributed to the good hydrophilicity of graphene. Moreover, one stronger absorption peak was found at 580 cm^{-1}, and this belongs to Fe-O-Fe stretching vibration, thereby showing that Fe_3O_4/Graphene oxide nanocomposite has been prapared with high purity.

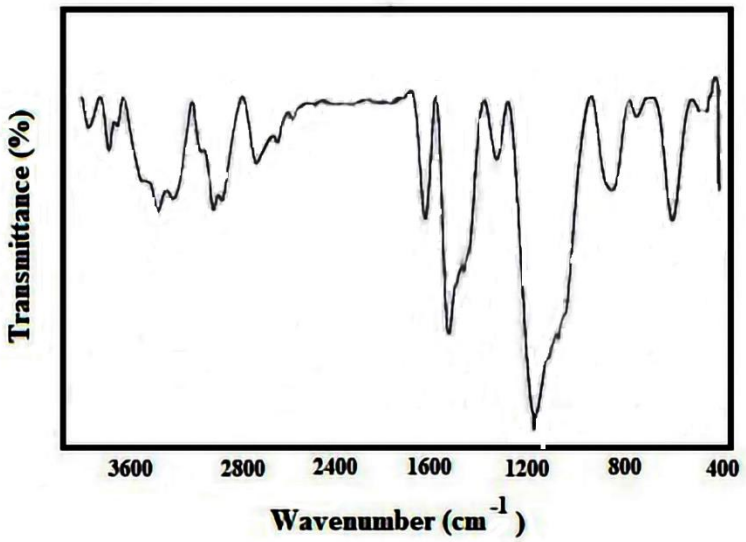

Fig. 3. FTIR spectrum ofFe_3O_4/Graphene oxide nanocomposite.

3.1.4 Elemental analysis with EDX spectroscopy

Energy dispersive X-ray spectroscopy analysis was applied to identify elements, which exist in the synthesized Fe_3O_4/Graphene oxide nanocomposite. C, O, and Fe peaks can be clearly seen from Fig. 4. Energy dispersive X-ray spectroscopy analysis demonstrated no significant levels of impurities, which could have originated from the procedure. Therefore, results of XRD, SEM, EDX, and FTIR imply the generation of Fe_3O_4/Graphene oxide .

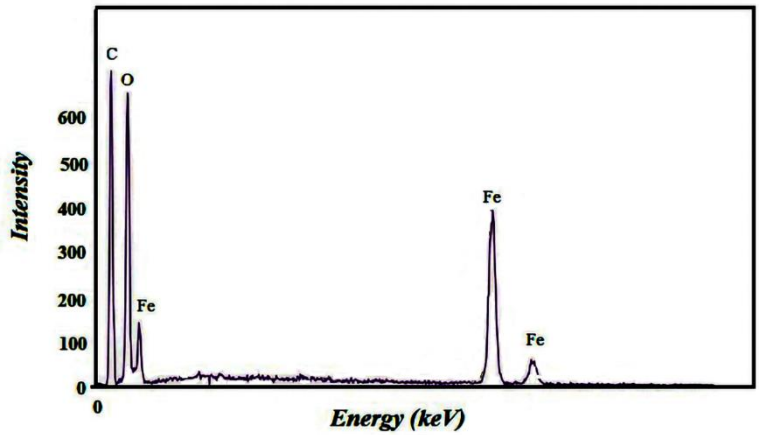

Fig. 4. EDX pattern of Fe_3O_4/Graphene oxide nanocomposite.

3.2 Photocatalytic activity

The efficiency of the prepared Fe_3O_4 and Fe_3O_4/Graphene oxide samples on the photocatalytic degradation of malachite green was studied in aqueous conditions against black light. The spectrum of blank sample that contain individual malachite green demonstrates absorption peak in the visible region located at wavelength of 620 nm. Based on results, the intensity of the absorption peak of malachite green declined upon enhancing illumination time. The related image of photocatalytic degradation of malachite green in the presence of Fe_3O_4 and Fe_3O_4/Graphene oxide under black light illumination are presented in Figs. 5. Fe_3O_4 nanoparticles can easily capture pollutant molecules and act as major catalytic species in the photocatalytic reactions. Furthermore, OH radicals generated during the reaction can positively affect the degradation procedure. The prepared Fe_3O_4/Graphene oxide was found to be more efficient at degrading completely tested pollutant compared to Fe_3O_4. It is known that the Fe_3O_4 decorated on both sides of Graphene sheets can enhance their specific surface area, which resulted in increased degradation of pollutant. Also, the high photocatalytic activity may be related to the conductive bonding of Fe_3O_4 on the Graphene, which may inhibit the recombination of photocreated electron–hole pairs. This mechanism is responsible for the increased degrading efficiency of Fe_3O_4/Graphene oxide compared to Fe_3O_4. During the photocatalytic procedure, malachite green was transformed into reactive, unstable intermediates and mineralized to colorless compounds. Electron–hole pairs in the excited Fe_3O_4 may be efficiently detached to enable an effective change into photoinduced electrons from Graphene sheet to Fe_3O_4 [18]. This essential electron transfer mechanism can play an important role in the elimination of pollutant molecules [19]. The efficiency of the photocatalytic activity depends on the effectiveness of the adsorption of unprocessed organic impurities on the catalysts and the route of excruciating photocreated electron–hole pairs [20]. It is concluded that the increased photocatalytic behavior of Fe_3O_4/Graphene oxide could play a vital role to solve environmental problems. As a result, the Fe_3O_4/Graphene oxide prepared in this work, possess a very efficient photocatalytic activity against dye molecules, showing their relevance for environmental remediation usage. The mechanism of photodegradation of malachite green over Fe3O4/Graphene oxide sample is depicted as following equations:

$$Fe_3O_4 + h\acute{u} \rightarrow h^+ (VB) + e^- (CB) \quad (4)$$

$$Graphene + h\acute{u} \rightarrow Graphene^- \quad (5)$$

$$Graphene + e^- (CB) \rightarrow Graphene^- \quad (6)$$

$$Graphene^- + O_2 \rightarrow Graphene + O_2^{\cdot -} \quad (7)$$

$$h^+ (VB) + H_2O \rightarrow H^+ + OH^{\cdot} \quad (8)$$

$$O_2^{\cdot -} + H^+ \rightarrow HO_2^{\cdot} \quad (9)$$

$$O_2^{\cdot -} + H^+ \rightarrow HO_2^{\cdot} \quad (10)$$

$$HO_2^{\cdot} + O_2^{\cdot -} + H^+ \rightarrow H_2O_2 + O_2 \quad (11)$$

$$H_2O_2 + e^- (CB) \rightarrow OH^- + OH^{\cdot} \quad (12)$$

$$OH^- + h^+ (VB) \rightarrow OH^{\cdot} \quad (13)$$

$$OH^{\cdot} + pollutant \rightarrow CO_2 + H_2O \quad (14)$$

However, in Fe_3O_4/Graphene oxide catalysts, the graphene amount is known as a vital factor in detecting the photocatalytic activity. The results of degradation of malachite green using Fe_3O_4/Graphene oxide catalysts with different graphene contents (Fe_3O_4/Graphene oxide$_1$, Fe_3O_4/Graphene oxide$_2$, Fe_3O_4/Graphene oxide$_3$ and Fe_3O_4/Graphene oxide$_4$) are illustrated in Fig. 5. From Fe_3O_4/Graphene oxide$_1$ to Fe_3O_4/Graphene oxide$_2$, the photocatalytic activity was gradually enhanced, and Fe_3O_4/Graphene oxide$_3$ showed the maximized photocatalytic activity. However, when the content of graphene is further enhanced, the photocatalytic performance declines. Graphene can absorb some black light and cause a light harvesting competition between and graphene. By enhancing of graphene amount, the photocatalytic activity is declined [23]. Furthermore, the excessive graphene may act as a kind of recombination center instead of providing an electron pathway and promote the recombination of photocreated electron-hole pair [24].

Fig. 6 demonstrates the UV-vis spectral changes of malachite green aqueous solution in the procedure of photodegradation by Fe_3O_4/Graphene oxide. From this figure, it is observed that, the absorbance at 620 nm of malachite green decreases gradually with time elapsed: which implies the reduction of malachite green from blue to colorless. The absorption peak completely disappeared in 15 min. The photograph of malachite green solution before and after black light illumination is given in Fig. 7 (inset), which also confirms the complete degradation of the malachite green.

3.3 Effect of the initial malachite green concentration in the Photocatalytic Reaction

The effect of varying malachite green initial concentration was investigated in the range of 10–40 mg L^{-1}. Figure 7 demonstrates a plot of ln (C_0/C) versus illumination time for all the experiments with various initial concentration of malachite green. The values of k_{obs} can be obtained by applying a least square regression analysis. By increasing the initial concentration of malachite green, more and more dye molecules can be adsorbed on the surface of Fe_3O_4/Graphene oxide. The high content of adsorbed dye is thought to have an

inhibitive influence on the reaction of dye molecules with photogenerated holes or OH radicals, due to the lack of any direct contact between them. This was related to the rise of internal optical density, which caused the solution to became impermeable to black light [25]. Once the concentration of dye is enhanced, it also causes malachite green molecules to absorb light and the photons never reach Fe_3O_4/Graphene oxide surface, and thus the photocatalytic degradation efficiency decreases [26, 27].

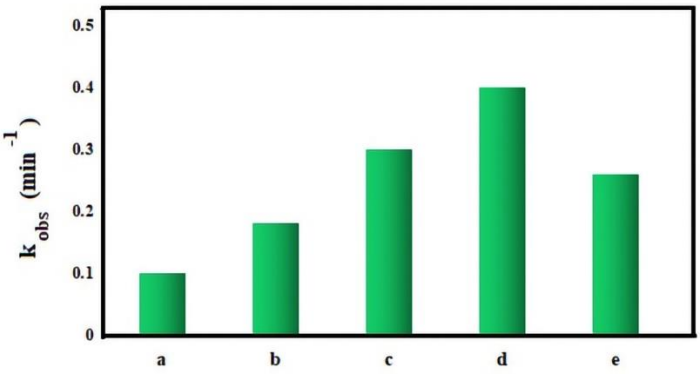

Fig. 5. Photocatalytic degradation of malachite green in the presence of (a) Fe_3O_4 , (b) Fe_3O_4/Graphene $oxide_1$, (c) Fe_3O_4/Graphene $oxide_2$, (d) Fe_3O_4/Graphene $oxide_3$, and (e) Fe_3O_4/Graphene $oxide_4$.

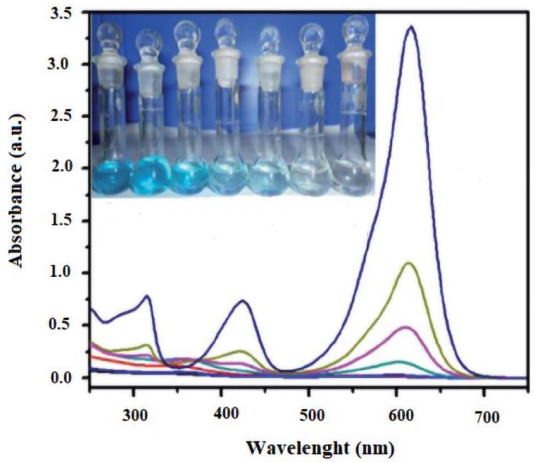

Fig. 6. UV-vis spectral changes and optical images (inset) of malachite green during degradation procedure as a function of reaction time using Fe_3O_4/Graphene oxide nanocomposite.

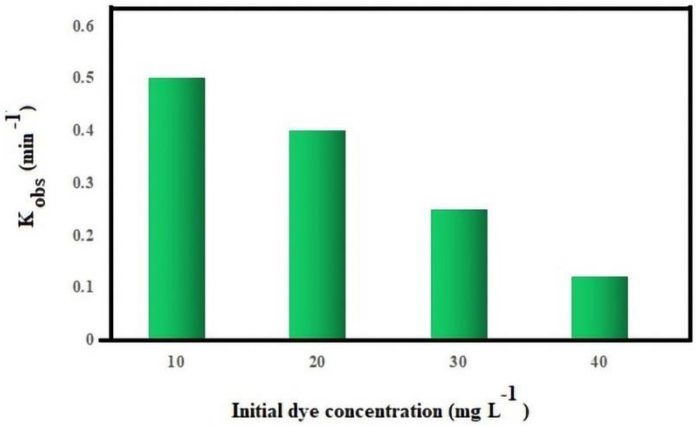

Fig. 7. Effect of initial dye concentration in the photocatalytic reaction.

It is well known that the heterogeneous photo-oxidation rate fits well to the classic Langmuir Hinshelwood (L-H) mechanism [26] which in terms of degradation kinetics can be explained as follows:

$$r = \frac{K_C\,(C)K_{dye}}{1 + (C_0)K_{dye}} \qquad (15)$$

$$\frac{1}{K_{obs}} = \frac{1}{K_C K_{dye}} + \frac{C_0}{K_C} \qquad (16)$$

where K_{dye} and K_C are the Langmuir-Hinshelwood adsorption equilibrium constant and rate constant of surface reaction, respectively [28]. Using the data from photocatalytic testts with various initial malachite green concentrations, the quantities of K_{dye} and K_C can be estimated via the linearized equation by plotting $1/K_{obs}$ versus $[C]_0$. From Fig. 8, a straight line fitted the experimental data reasonably well (the coefficient of linear regression, r, was 0.996), thus implying that photocatalytic degradation of malachite green most probably follows Langmuir-Hinshelwood kinetics. From the slope of the straight line, K_C was computed equal to 2.32 mg L^{-1} min^{-1}, while from the intercept, K_{dye} was 0.91 $(mg\ L^{-1})^{-1}$.

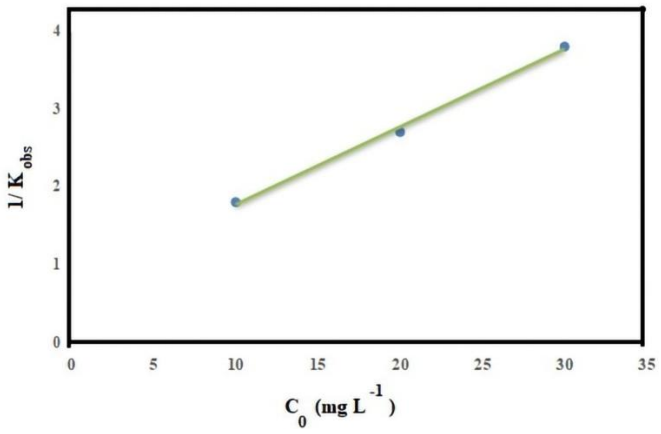

Fig. 8. Determination of the adsorption equilibrium constant, K_{dye} and K_C, for the Langmuir-Hinshelwood kinetic model.

3.4 Sonodegradation of malachite green by prepared nanocompounds

The degradation rate of malachite green was investigated via exposing the dye solution to ultrasonication in the absence and in the presence of prepared Fe_3O_4/Graphene oxide. Malachite green undergoes few degradation under direct ultrasonic radiation in the absence of Fe_3O_4/Graphene oxide nanocompposite. This may be attributed to the low rate of hydroxyl radical production via sonolysis alone. However, the presence of Fe_3O_4/Graphene oxide showed excellent results as a sonocatalyst in the degradation of malachite green (Figure 9). This phenomenon can be related to the enhanced number of cavitation bubble which occurs on the surface of Fe_3O_4/Graphene oxide and yielded in water cleavage and generation of excess hydroxyl radicals [29-30]. Furthermore, the fast degradation of malachite green via sonocatalytic procedure in the presence of Fe_3O_4/Graphene oxide can be attributed to the sonoluminescence mechanism. Sonoluminescence involves an intense UV-light, which promotes Fe_3O_4/Graphene oxide nanocomposite to act as an efficient photocatalyst during ultrasonic radiation [31]. The sonodegradation mechanism of malachite green on Fe_3O_4/Graphene oxide can be expressed as follows:

The chemical effects of ultrasound include the process of cavitation which is the nucleation, growth, and collapse of bubbles in a liquid [32]. The collapse of the bubbles induces high-energy phenomena, i.e., high temperature and pressure (~5000 K and 500 bars), electrical discharges, and plasma influences. The consequences of these extreme conditions are the direct thermal dissociation (sonolysis) of dissolved oxygen and water molecules into highly reactive radical species:

$$H_2O \xrightarrow{US/sonolysis} H^{\cdot} + OH^{\cdot} \qquad (17)$$

$$O_2 \xrightarrow{US/sonolysis} 2\,O^{\cdot} \qquad (18)$$

$O_2^{\cdot}$ can react with water molecules to form $OH^{\cdot}$:

$$H_2O + O^{\cdot} \rightarrow 2\,OH^{\cdot} \qquad (19)$$

Furthermore, sonochemistry also includes the emission of light energy for a small period of time. The illumination can lead to the photoexcitation of electrons from the valence band to the conduction band, thus leading to the production of electron-hole pairs in a similar manner as described above for the photocatalysis [33]. Hydroxyl radicals with high oxidizing activity can more react with malachite green and degrade it into small

species. The organic pollutant decomposition mechanism involved:

*Adsorption, the electrostatic attraction between graphene and malachite green molecules

**Sonocatalysis, the sonocatalytic degradation of malachite green by ultrasonic radiation began with excitation of Fe_3O_4 and formation of electron-hole pairs. High oxidation valence-band holes can oxidize dye molecules. Water degradation or reaction of h^+ with OH can form hydroxyl radicals. Meanwhile, the reaction between conduction-band electrons (e^-) and proper electron acceptors (such as O_2) yielded oxidative radicals. The produced hydroxyl radicals can easily degraded dye molecules [31].

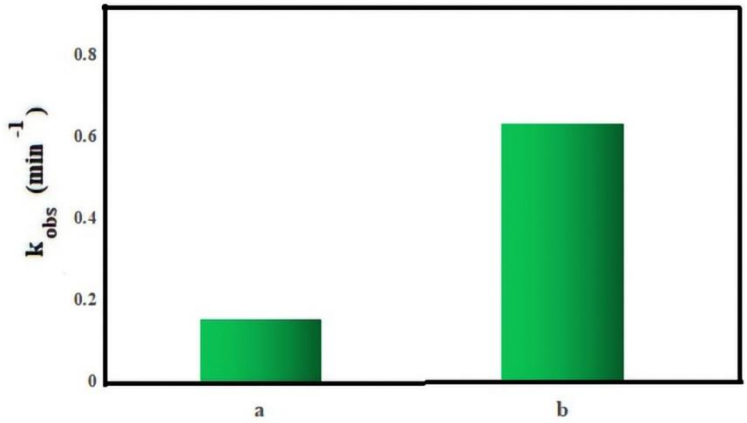

Fig. 9. Sonocatalytic degradation of malachite green in the presence of (a) US only, (b) Fe_3O_4/Graphene oxide.

3.5 Comparison of Efficiency of Photocatalysis and Sonocatalysis of Fe_3O_4/Graphene oxide nanocomposite

The degradation rate of malachite green via photolysis and sonolysis process in the presence of Fe_3O_4/Graphene oxide nanocomposite is illustrated in Fig. 10. It can be observed that sonodegradation procedure is faster than photodegradation process. Therefore, US radiation is a better source than UV-visible radiation for the degradation of malachite green in the presence of Fe_3O_4/Graphene oxide nanocomposite. Fe_3O_4 nanoparticles have a lower band gap (2.2 eV). So, electron-hole recombination is faster and easier. Therefore, the formation of $OH^{\cdot}$ is hard, which results in lower degradation of malachite green in the case of photocatalysis. In the presence of Fe_3O_4/Graphene oxide nanocomposite, the sonodegradation rate of pollutant was enhanced. This is due to synergistic influences of ultrasound and solid catalyst, namely [34-35], (1) added materials could provide additional nuclei for cavitation bubble formation, (2) US radiation enhances the mass transfer of malachite green between the liquid phase and Fe_3O_4/Graphene oxide nanocomposite surface, (3) US radiation increases the active surface area due to ultrasound disaggregating, and (4) the catalyst can be promoted by ultrasoundinduced luminescence which has a wide wavelength. This phenomenon can increase the formation of $OH^{\cdot}$ in the reaction mixture. Therefore, sonocatalysis can enhance the degradation rate of pollutants.

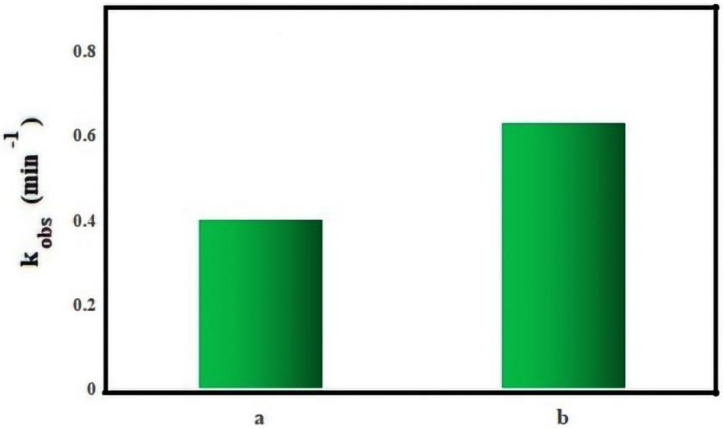

Fig. 10. Degradation rates of malachite green under (a) UV-visible radiation and (b) US radiation.

4. Conclusion

Fe_3O_4, and Fe_3O_4/Graphene oxide were synthesized and employed as catalysts for the photodegradation and sonodegradation of malachite green. The results of the XRD, SEM, FT-IR, and EDX analyses showed that the synthesis of samples was carried out successfully. The effect of graphene on the photoinduced charge property was investagated. It is concluded that Fe_3O_4/Graphene oxide nanocomposite is more effective in the comparison with Fe_3O_4 photocatalyst because of increasing in the specific surface area, and decreasing in the recombination rate of photocreated electron–hole pairs. The photocatalytic degradation was obviously affected by the initial concentration with respect to Langmuir-Hinshelwood kinetic model. Langmuir-Hinshelwood kinetic model provided a good fit to the photocatalytic degradation of malachite green, used in this study. Based on results, the photocatalytic degradation of malachite green via Fe_3O_4/Graphene oxide nanocomposite needs more time. The synergistic effect of Fe_3O_4/Graphene oxide nanocomposite and sonocatalysis has been showed to be more effective in degrading malachite green as compared to Fe_3O_4/Graphene oxide nanocomposite and photocatalysis. Sonocatalytic degradation of malachite green in the presence of Fe_3O_4/Graphene oxide nanocomposite could be explained by the mechanisms of hot spots and sonoluminescence. This research confirms the potentialities of heterogeneous photocatalysis to decontaminate wastewaters containing organic pollutants.

Acknowledgments

The author acknowledges the support of Payame Noor University of Iran.

References

[1] B.D. Deshpande, P.S. Agrawal, M.K.N. Yenkie, J.S. Dhoble, Prospective of Nanotechnology in Degradation of Waste Water: A New Challenges, Nano-Struct. Nano-Objects., 22 (2020) 100442.

[2] S. A. Siadati, M. A. Ebrahimzadeh, R. Yazdian- Robati, E. Babanezhad, A theoretical approach on the possibility of using α-phographene, g-X3N4 nanosheets, and C19X fullerenes for adsorption and drug delivery of a proteasome inhibitor drug, Diam. Relat. Mate., 147 (2024) 111344.

[3] N. Zare Davijani, R. Kia-Kojoori, S. Abdolmohammadi, S. Sadegh-Samiei, Ultrasonic-assisted synthesis of highly effective visible light Fe3O4/ZnO/PANI nanocomposite: Thoroughly kinetics and thermodynamic investigations on the Congo red dye decomposition, Mol. Struct., 1250 (2022) 131903.

[4] S. FakheriVayeghan, S. Abdolmohammadi, R. Kia-ojoori, An expedient synthesis of 6- amino-5-[(4-hydroxy-2-oxo-2H-chromen-3-yl)(aryl)methyl]-1,3-dimethyl,4,6(1H,3H)- pyrimidinedione derivatives using Fe3O4@TiO2 nanocomposite as an efficient, magnetically separable, and reusable catalyst, Z. Naturforsch. B., 73 (2018) 545-551.

[5] F. Chaghari-Farahani, S. Abdolmohammadi, R. Kia-Kojoori, PANI-Fe3O4@ZnO nanocomposite: A magnetically separable and applicable catalyst for the synthesis of chromeno-pyrido[d]pyrimidine derivatives. RSC Adv., 10 (2020) 15614-15621.

[6] R. Mohammadi, Influence of preparation method on the physicochemical properties and catalytic activity of SiO2–TiO2 mixed oxides, Desal. Wat. Treat., 57 (2016) 23370–23377 .

[7] S. Abdolmohammadi, B. Mirza, E. Vessally, Immobilized TiO2 nanoparticles on carbon nanotubes: An efficient heterogeneous catalyst for the synthesis of chromeno[b]pyridine derivatives under ultrasonic irradiation. RSC Adv., 9 (2019) 41868-41876.

[8] V.L.E. Siong, K.M. Lee, J.C. Juan, C.W. Lai, X.H. Tai, C.S. Khe, Removal of methylene blue dye by solvothermally reduced graphene oxide: a metal-free adsorption and photodegradation method, RSC Adv., 9(2019) 37686–37695.

[9] S.X. Wang, H. Maimaiti, B. Xu, A. Awati, G.B. Zhou, Y.D. Cui, Synthesis and visible light photocatalytic N2/H2O to ammonia of ZnS nanoparticles supported by petroleum pitch-based graphene oxide, Appl. Surf. Sci., 493 (2019) 514–524.

[10] N. Asadi, Synthesis, characterization and in vitro evaluation of magnetic nanoparticles modified with PCL–PEG–PCL for controlled delivery of 5FU, Art Cells, Nanomed, and Biotechnol., 2018:1–8 (2018).

[11] T.A. Abdullah, T. Juzsakova, R.T. Rasheed, A.D. Salman, V. Sebestyen, E. Domokos, B. Sluser, Cretescu, Polystyrene-Fe3O4-MWCNTs Nanocomposites for Toluene Removal from Water., Materials., (2021) 5503-5523.

[12] S. Ebrahimiasl, F. Behmagham, S. Abdolmohammadi, R. Kojabad, E. Vessally, Recent advances in the application of nanometal catalysts for Glaser coupling, Curr. Org. Chem., 23 (2019) 2489-2503.

[13] S. Abdolmohammadi, M. Afsharpour, An ultrasound assisted cyclocondensation reaction for the efficient synthesis of [1]benzopyranopyrido[d]pyrimidines using porous graphene/MoO3. Appl. Organomet. Chem., 35 (2021) e6028.

[14] M. Ebrahimi, S. Abdolmohammadi, R. Kia-Kojoori, Ultrasonic accelerated efficient synthesis of aminobenzochromenes using Ag2Cr2O7 nanoparticles as a reusable heterogeneous catalyst. J. Heterocycl. Chem., 57 (2020) 1875-1881.

[15] B. Saeedi, S. Abdolmohammadi , Z. MirJafari, R. Kia-Kojoori, Nickel(II) chromite nanoparticles: An eco-friendly and reusable catalyst for synthesis of 2,4-diamino-6-aryl-pyrimidine-5-yl cyanides under

ultrasonic radiation. Comb. Chem. High Throughput Screen., 24 (2021) 455-464.

[16] A.M. Tayler, R. Farouq, O.A. Mohamed, M.A. Tony, Oil spill clean-up using combined sorbents: A comparative investigation and design aspects, Int. J. Environ. Anal. Chem., 100 (2020) 311–323.

[17] Abdolmohammadi S., Shariati S., Elmi Fard N., Samani A., Aqueous-mediated green synthesis of novel spiro[indole-quinazoline] derivatives using Kit-6 mesoporous silica coated Fe3O4 nanoparticles as catalyst, J. Heterocycl. Chem., 57 (2020) 2729-2737.

[18] M. Pleguezuelos-Villa, A. Nácher, M.J. Hernández, M.A. Ofelia Vila Buso, A. Ruiz Sauri, O. Díez-Sales, Mangiferin nanoemulsions in treatment of inflflammatory disorders and skin regeneration. Int. J. Pharm., (2019) 299–307.

[19] R.K. Khurana, B.L. Gaspar, G. Welsby, O.P. Katare, K.K. Singh, B. Singh, Improving the biopharmaceutical attributes of mangiferin using vitamin E-TPGS co-loaded self-assembled phosholipidic nano-mixed micellar systems, Drug Deliv. Transl. Res., 8 (2018) 617–632.

[20] A. Goł ˛abiewska, M. Paszkiewicz-Gawron, A. Sadzi ´nska, W. Lisowski, E. Grabowska, A. Zaleska-Medynska, J. Łuczak, Fabrication and photoactivity of ionic liquid–TiO2 structures for efficient visible-light-induced photocatalyticdecomposition of organic pollutants in aqueous phase, Beilstein J. Nanotechnol., 9 (2018) 580–590.

[21] R. Mohammadi, B. Massoumi, F. Galandar, Polyaniline-TiO2 /graphene nanocomposite: an efcient catalyst for the removal of anionic dyes, Desal. Wat. Treat., 142 (2019) 321–330.

[22] J. Łuczak, M. Paszkiewicz-Gawron, M. Długok ˛ecka, W. Lisowski, E. Grabowska, S. Makurat, J. Rak, Zaleska-Medynska, Visible light photocatalytic activity of ionic liquid-TiO2 spheres: Effect of the ionic liquid's anion structure, Chem.Cat.Chem., 9 (2017) 4377–4388.

[23] O.A.A. El-Shamy, R.E. El-Azabawy, O.E. El-Azabawy, Synthesis and Characterization of Magnetite-Alginate Nanoparticles for Enhancement of Nickel and Cobalt Ion Adsorption from Wastewater, J.Nanomaterials., 2019: Article ID 6326012, 8 pages.

[24] A.M. Al-Sabagh, Y.M. Moustafa, A. Hamdy, H.M. Killa, R.T.M. Ghanem, R.E. Morsi, Preparation and characterization of sulfonated polystyrene/magnetite nanocomposites for organic dye adsorption, Egypt. J.Pet., 27 (2018) 403–413.

[25] N.S. Rajurkar, D. Mahajan, Adsorption of cobalt (II) and nickel (II) ions from aqueous solution on chitosan, 6 (2016) 1203–1217.

[26] N. Pervez, W. He, T. Zarra, V. Naddeo, Y. Zhao, New Sustainable Approach for the Production of Fe3O4/Graphene Oxide-Activated Persulfate System for Dye Removal in Real Wastewater, Water., 12(2020) 733-750.

[27] X. Cheng, H. Guo, Y. Zhang, X. Wu, Y, Liu. Non-photochemical production of singlet oxygen via activation of persulfate by carbon nanotubes, Water. Res., 113 (2017) 80–88.

[28] X. Wang, Y. Qin, L. Zhu, H. Tang, Nitrogen-doped reduced graphene oxide as a bifunctional material for removing bisphenols: Synergistic effffect between adsorption and catalysis., Environ. Sci. Technol., 49 (2015) 6855–6864.

[29] S. Sarkar, N. T. Ponce, A. Banerjee, R. Bandopadhyay, S. Rajendran, E. Lichtfouse, Green polymeric nanomaterials for the photocatalytic degradation of dyes: a review, Environ. Chem. Lett., 18 (2020) 1569–1580.

[30] V.K. Nathan, P. Ammini, J. Vijayan, Photocatalytic degradation of synthetic dyes using iron (III) oxide nanoparticles (Fe2O3 -Nps) synthesised using Rhizophora mucronata Lam, IET Nanobiotechnol., 13 (2019) 120-123.

[31] S. Abdolmohammadi, S. Shariati, B. Mirza, Ultrasound promoted and Kit-6 mesoporous silica supported Fe3O4 MNPs catalyzed cyclocondensation reaction of 4-hydroxycoumarin, 3,4-methylenedioxyphenol and aromatic aldehydes, Appl. Organomet. Chem., 35 (2021) e6117.

[32] S.D. Abraham, S.T. David, R.B. Bennie, Eco-friendly and green synthesis of BiVO4 nanoparticle using microwave irradiation as photocatalayst for the degradation of Alizarin Red S, J. Mol. Struct., 1113 (2016) 174–181.

[33] A. Alshehri, M.A. Malik, Z. Khan, Biofabrication of Fe nanoparticles in aqueous extract of Hibiscus sabdariffa with enhanced photocatalytic activities, RSC Adv., 7 (2017) 25149–25159.

[34] R. Mohammadi, B. Massoumi, R. Mashayekhi, Fe3O4/polystyrene-alginate nanocomposite as a novel adsorbent for highly efficient removal of dyes, J. Chem. Chem. Eng. *(IJCCE).*, Article in press.

[35] R. Mohammadi, Highly Efficient catalyst of TiO2/chitosan for Photodegradation and Sonodegradation of Organic Pollutants, Chem. Rev. Lett., 5 (2022) 133-140.